Impact of Mesoscale Momentum Transport on Large-Scale Tropical Dynamics: Linear Analysis of the Shallow-Water Analog

JUN-ICHI YANO

CRC-SHM, Monash University, Clayton, Victoria, Australia

MITCHELL W. MONCRIEFF

National Center for Atmospheric Research, Boulder, Colorado*

(Manuscript received 11 June 1996, in final form 14 July 1997)

ABSTRACT

The vertical transport of horizontal momentum by organized convection is a prominent process, yet its impact on the large-scale atmospheric circulation has not even been qualitatively assessed. In order to examine this problem in a simple framework the authors incorporate a nonlinear dynamical model of convective momentum flux into a linear model of the large-scale tropical atmosphere. This model has previously been used to investigate the WISHE (wind-induced surface-heat exchange) instability.

In order to implement the dynamically determined fluxes as a parameterization, a closure assumption is required to relate the relevant mesoscale parameters to the large-scale variables. The most straightforward method is to relate the low-level large-scale pressure (p_L) to the mesoscale pressure perturbation (p_M), which is linked to the mesoscale momentum flux by the dynamical model. The mesoscale momentum transport under this closure reduces the effective pressure gradient in the large-scale momentum equation and, consequently, the effective stratification. A sufficiently large p_M may even cause an effectively unstable stratification (convective instability by mesoscale momentum transport), which is marginally realizable according to a scale analysis.

In general, the WISHE instability is suppressed by the mesoscale momentum flux under this closure because a larger effective stratification can provide a more efficient mass redistribution and, in turn, a larger potential energy for WISHE. This demonstrates that momentum transport by mesoscale convective systems can substantially modify the large-scale tropical dynamics through the WISHE mechanism.

1. Introduction

Although organized convection on scales of tens to hundreds of kilometers (mesoscales) is a well-recognized atmospheric process, the impact of the accompanying momentum transport on the large scales of motion is poorly understood and has not been much studied. The purpose of this paper is to investigate, at a fundamental level, the large-scale response of the tropical atmosphere to momentum transport by the most highly organized regime of deep convection, namely, squall lines. These systems are quite common in certain regions or, in more basic terms, in certain types of environmental shear. We recognize that they have an impact on quantities other than the momentum field because they transport large quantities of mass. For example, mass transport strongly affects the mean thermodynamic and moisture profiles (Lafore et al. 1988). Note that the redistribution and generation of upper-tropospheric moisture through the cirrus and stratiform outflow in highly organized convective systems strongly affects the radiative fluxes, which is important to climate. However, we choose to focus on the aspects pertaining to the organized momentum flux for the reasons stated above.

A series of field experiments and accompanying studies reviewed, for example, in Houze and Betts (1981), Houze (1989), Rutledge (1991), and Moncrieff (1995) has shown that mesoscale convective systems are commonly organized into squall lines in both Tropics and midlatitudes. The most subtle effect of these systems on the large scale is arguably through the vertical transport of the momentum. Unlike the effect of cumulus, in which only the ensemble effects of *thermodynamic* processes on the large-scale dynamics have been traditionally considered, the organized flow associated with squall line convection causes a distinctive momentum transport. This dynamical aspect of mesoscale organization is a process not yet accounted for in global

* The National Center for Atmospheric Research is sponsored by the National Science Foundation.

Corresponding author address: Dr. Jun-Ichi Yano, CRC-SHM, Monash University, 3rd floor, Building 70, Wellington Rd., Clayton, Victoria 3168, Australia.
E-mail: jiy@vortex.shm.monash.edu.au

models. Various basic aspects of the momentum transport problem are presented in Moncrieff (1997), including the various kinds of momentum transport and a dynamical basis for the concept of organized convection.

Regimes of organized convection and the accompanying momentum fluxes were derived analytically by Moncrieff (1981) using nonlinear idealized models. Motivated to reduce the squall line regime to first principles for purposes of parameterization, Moncrieff (1992, hereafter M92) derived a steady-state dynamical model that was a paradigm of the observationally based conceptual model of Houze et al. (1989). This model, which contains no explicit heating, is the simplest possible (archetypal) realization of the mass and momentum fluxes by squall lines.

The archetypal model is characterized by three quantities (cf. Fig. 1 of M92), namely, the normalized pressure change (or jump) across the convective system (E_M), the inflow depth of the front-to-rear flow (h_0), and the mesoscale downdraft depth (h). The conservation of Bernoulli energy, mass, and other properties, as well as continuity of pressure provide a one-to-one relationship among these three parameters. If one parameter is specified, then both the momentum flux and the vertical mass flux can be obtained in a consistent manner.

Liu and Moncrieff (1996) showed that neither the ambient stratification nor the latent heat release has much effect on the archetypal momentum fluxes. In addition, LeMone and Moncrieff (1994) evaluated these fluxes against observations and Wu and Moncrieff (1996) carried out comparison against numerical model results. These studies demonstrated that the archetypal model is a plausible paradigm for the momentum flux, not only by squall lines but also by similar kinds of flow-perpendicular systems such as cold-frontal rainbands and gust fronts of smaller scale.

With the validity of the model reasonably well established, we take the next step to incorporate the flux theory into a momentum parameterization for the large-scale equations. This warrants special attention because organized deep convection can occur on a scale comparable to the grid scale of global models. This creates the odd situation that organized convective systems are neither fully resolved nor sufficiently small to be adequately parameterized as a subgrid-scale process. For example, a supercluster (which can be thought of as a giant mesoscale convective system) that occurred during the December 1992 westerly wind burst during TOGA COARE was analyzed by Moncrieff and Klinker (1997). They identified a new uncertainty in a high-resolution, state-of-the-art weather prediction model having a grid length of about 90 km. This uncertainty sprung from a surrogate treatment of a supercluster as a single physical entity rather than an ensemble of mesoscale convective systems and convection that it really represents. This surrogate process caused errors in the convective momentum flux that directly affected the large-scale flow.

The motivation for this inaugural study of the large-scale impact of momentum flux is to seek a simple physical interpretation; therefore we adopt an idealized approach rather than implement the parameterization into a general circulation model (GCM). Specifically, we use the shallow-water model of Yano and Emanuel (1991, hereafter YE) as an idealization of the large-scale tropical atmosphere. The model has a standard bulk surface flux and bulk mass flux formulation for thermodynamics and a closure based on a convective quasi-equilibrium assumption. The modification of the wind-induced surface heat exchange (WISHE) instability for the large-scale tropical circulation by convective downdrafts was analyzed by YE using this model. WISHE was proposed by Emanuel (1987) and Neelin et al. (1987) as a theory for Madden–Julian waves, as an alternative to wave-CISK (cf. Emanuel et al. 1994). The model was also used to investigate other aspects of tropical dynamics (Yano et al. 1995, 1996). It was recently used to compare the impact of several parameterization categories (Yano et al. 1997) on the tropical atmosphere.

We extend the original shallow-water formulation of the model to a two-layer framework. This enables us to explicitly investigate the transport of horizontal momentum by mesoscale convection from the lower to the upper level (i.e., between lower and upper troposphere). Note that the momentum flux has a strong bimodal signature characterized by accelerations of opposing sign in the low and upper troposphere. We specifically enquire, how is the WISHE instability modified by mesoscale momentum transport and how does this affect the large-scale tropical dynamics? We address this question using a linear stability analysis that incorporates Moncrieff's archetypal model of the mesoscale momentum transport.

To close the parameterization, the archetypal mesoscale momentum transport must be somehow linked to the large-scale (predicted) variables. In evaluating the archetypal model from observations, LeMone and Moncrieff (1994) chose the inflow depth h_0 as a reference parameter in order to compare the archetypal momentum transport with observational data. In our study, we choose the mesoscale pressure jump E_M as a simple closure. Because E_M is functionally related (through the archetypal model) to the mesoscale change of pressure across the mesoscale system, it is reasonable to assume that it is continuous with the pressure change due to the large-scale wave response ($\delta\phi$). This closure will be presented in section 3.

As an illustration of a relevant large-scale setting we refer to the studies of the global distribution and frequency of organized mesoscale convective systems by Laing and Fritsch (1997). Their results illustrate that, rather than being uniformly distributed, large organized precipitating systems tend to be concentrated in specific regions and occur during specific periods, for example, during the Indian monsoon, in West Africa, and in Venezuela. We stress that these regions are characterized

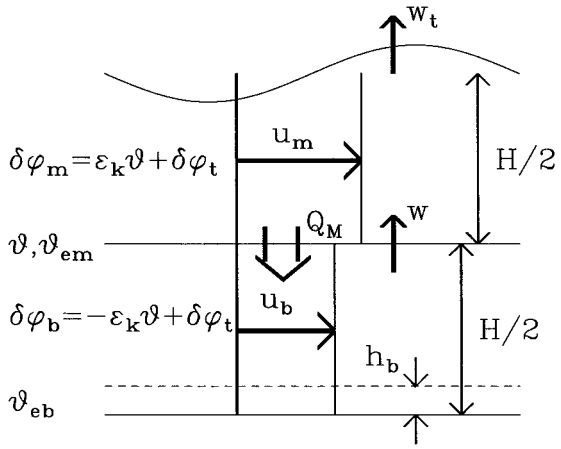

FIG. 1. Model configuration.

by jetlike wind profiles and moderate-to-strong low-tropospheric shear. Jetlike profiles are known to be associated with squall line cloud systems. For example, Lafore and Moncrieff (1989) conducted a systematic numerical study of the effect of jetlike profiles on West African squall lines. Moreover, studies during TOGA COARE indicate that large-scale circulations such as Madden–Julian waves (Madden and Julian 1971) contain an ensemble of organized mesoscale systems, a behavior seen during westerly wind bursts in the previously cited Moncrieff and Klinker (1997) analysis (see their Figs. 1 and 2). Taking the TOGA COARE situation as an example, we assume a westerly mean wind in the linear stability analysis. The results can be simply transformed to apply to an easterly mean state.

In the following section we describe the basic formulation of the large-scale model. This is followed by a summary of the mesoscale momentum flux parameterization in section 3. Section 4 is devoted the shallow-water limit of the two-layer system. Finally, conclusions are summarized in section 5.

2. Basic formulation

a. Two-layer system

We use the idealized large-scale tropical model formulation of Yano and Emanuel (1991) extended to a two-layer system. In order to simplify the mathematical analysis we ignore planetary rotation and thereby retain only the horizontally one-dimensional Kelvin-like modes (Yano and Emanuel 1991); that is, a Rossby wave response cannot occur. We use two distinct types of parameterization. First, the mass flux formulation introduced by YE primarily represents the *thermodynamic* effect of cumulus convective scales. Second, we incorporate Moncrieff's archetypal model of mesoscale momentum transport. For simplicity, neither the momentum transport by cumulus nor the thermodynamic effects of mesoscale convection are considered. Although the latter effect is potentially important, its investigation is beyond the scope of this paper.

The model consists of two layers each of depth $H/2$, which corresponds to about 4 km on a density-weighted height scale (Fig. 1). The bottom of the lower layer contains the subcloud layer of depth $h_b = 500$ m. We assume a vertically homogeneous potential temperature so that $\theta = \theta(x, y)$. An equivalent potential temperature (θ_e) is assigned to the subcloud layer and another to the middle level of the troposphere. We identify variables in these layers by the subscripts b and m, respectively.

The vertical discretization of the model is obtained by vertically integrating the hydrostatic equation $\partial(\delta\phi)/\partial p = -\delta\alpha$ from the top of the subcloud layer to an arbitrary level. The variables ϕ and α are the geopotential and the specific volume, respectively, and δ designates a deviation from the mean value on a constant pressure surface. In integrating the right-hand side, we relate the specific volume α to the potential temperature θ by $\delta\alpha = (\partial\alpha/\partial\theta_e^*)_p\delta\theta_e^*$, $(\partial\alpha/\partial\theta_e^*)_p = C_p/\theta_0(\partial T/\partial p)_{\theta_e^*}$, and $\delta\theta_e^* = \gamma\delta\theta$, where θ_e^* is the saturated equivalent potential temperature, C_p is the specific heat at constant pressure, $\theta_0 = 300$ K is the reference potential temperature (a surface value), and $\gamma = \Gamma_d/\Gamma_m$ is the ratio of the dry adiabat to the moist adiabat. (See appendix A for definition of symbols.)

We define T and T_b as the temperature at an arbitrary level and the top of the subcloud layer, respectively. We then obtain

$$\delta\phi - \delta\phi_b = -\frac{\gamma C_p}{\theta_0}(T - T_b)\delta\theta. \tag{2.1}$$

Averaging of (2.1) over the model troposphere gives

$$\delta\phi_b = -\epsilon_k\delta\theta + \delta\phi_t, \tag{2.2a}$$

where

$$\epsilon_k = \frac{\gamma C_p}{\theta_0}(T_b - T_t) \approx 1.7 \times 10^2 \text{ J K}^{-1} \text{ kg}^{-1} \tag{2.2b}$$

and the subscript t designates a tropospheric mean. The potential temperature anomaly will generate a baroclinic mode of the same magnitude but of opposite sign in these layers. The mean geopotential $\delta\phi_t$ contributes solely to the barotropic mode. The midlevel geopotential

$$\delta\phi_m = \epsilon_k\delta\theta + \delta\phi_t \tag{2.2c}$$

is obtained from (2.1) by assuming $T_t = (T_b + T_m)/2$.

The potential temperature fluctuation is obtained from the thermodynamic equation

$$\frac{D_t}{Dt}\delta\theta = -\frac{N^2}{g}\theta_0 w + \dot{Q}_{\text{conv}} - \dot{Q}_R, \tag{2.3}$$

where

$$\frac{D_t}{Dt} \equiv \frac{\partial}{\partial t} + \mathbf{v}_t\cdot\nabla \tag{2.4}$$

represents the Lagrangian time derivative advected by

a mean tropospheric wind $\mathbf{v}_t \equiv (\mathbf{v}_b + \mathbf{v}_m)/2$, where $\mathbf{v}$ is a *horizontal* vector. The first term on the right-hand side of (2.3) represents adiabatic heating due to the vertical motion w, where $N = 10^{-2}$ s^{-1} is the Brunt–Väisälä frequency and $g = 9.8$ m s^{-2} the acceleration of gravity. We assume that the parameterized heating ($\dot{Q}_{\text{conv}}$) by cumulus convection is exactly balanced by adiabatic cooling, in accordance with a standard mass flux formulations (cf. Yanai and Johnson 1993). We can therefore write

$$\dot{Q}_{\text{conv}} = \frac{N^2}{g}\theta_0 w_c, \tag{2.5a}$$

where w_c is the *total* cumulus updraft given as a grid domain average.[1] The radiative cooling is represented using a Newtonian approximation,

$$\dot{Q}_R = \dot{Q}_{R_0} + \frac{\theta}{\tau_R}, \tag{2.5b}$$

with $\dot{Q}_{R0} = 1$ K day^{-1} and $\tau_R = 50$ days.

We assume a Klemp and Durran (1983) gravity wave radiation condition at the free upper boundary. Note that, since rotational modes are omitted, the barotropic mode cannot exist without a free surface. It follows that

$$\delta\phi_m = \frac{N}{k} w_t, \tag{2.6}$$

where w_t is the vertical velocity at the tropopause, k is the horizontal wavenumber, and $\delta\phi_m$ is defined by (2.2c).

Mass continuity follows from the incompressible approximation integrated from the bottom to top of each layer:

$$\frac{H}{2}\nabla\cdot\mathbf{v}_b + w = 0, \tag{2.7a}$$

$$\frac{H}{2}\nabla\cdot\mathbf{v}_m + w_t - w = 0. \tag{2.7b}$$

For simplicity we have assumed that the wind speed is uniform in each layer ($\mathbf{v}_b$ and $\mathbf{v}_m$, respectively). The equation of motion for each layer is given by

$$\frac{D_b}{Dt}\mathbf{v}_b = -\nabla\delta\phi_b + Q_M - \frac{1}{h_b}C_D|\mathbf{v}_b|\mathbf{v}_b, \tag{2.8a}$$

$$\frac{D_m}{Dt}\mathbf{v}_m = -\nabla\delta\phi_m - Q_M, \tag{2.8b}$$

where the surface drag coefficient $C_D = 1 \times 10^{-3}$ and the Lagrangian time derivatives are

$$\frac{D_b}{Dt} \equiv \frac{\partial}{\partial t} + \mathbf{v}_b\cdot\nabla, \tag{2.9a}$$

$$\frac{D_m}{Dt} \equiv \frac{\partial}{\partial t} + \mathbf{v}_m\cdot\nabla. \tag{2.9b}$$

Assuming that the momentum fluxes are zero at top and bottom, the redistribution of horizontal momentum (Q_M) by the mesoscale circulation has the same mean value, but the opposite sign, in each layer [see Moncrieff 1992, Eq. (15)]. Quantification of the large-scale effects of this redistribution of momentum is our primary aim. The detailed expression for Q_M is derived in section 3.

Moist thermodynamics are described by

$$h_b\frac{D_b}{Dt}\theta_{eb} = E - D, \tag{2.10a}$$

$$H\frac{D_m}{Dt}\theta_{em} = D - H\dot{Q}_R, \tag{2.10b}$$

with the surface heat flux E and the downdraft D given by bulk formulas

$$E = C_\theta|\mathbf{v}_b|(\theta^*_{eb} - \theta_{eb}), \tag{2.11a}$$

$$D = (w_d - w_e)(\theta_{eb} - \theta_{em}), \tag{2.11b}$$

where $C_\theta = 1.2 \times 10^{-3}$ is the evaporation rate and θ^*_{eb} the saturated potential temperature of the subcloud layer. The convective downdraft

$$w_d \equiv (1 - \epsilon_p)w_c/\epsilon_p \tag{2.11c}$$

is assumed to be consistent with a constant ''precipitation efficiency'' $\epsilon_p = 0.9$. The environmental subsidence is

$$w_e \equiv w - w_c. \tag{2.11d}$$

Note that w_d and w_e are grid averages, like w_c (see fn 1).

The precipitation efficiency ϵ_p measures the rate at which total water reaches the surface, by which we mean water generated by both cumulus-scale and mesoscale processes. Since the highest precipitation rate is due to the cumulus-scale processes, the precipitation efficiency is taken to be $\epsilon_p = 0.9$ by weighting toward convective precipitation. As a result, $1 - \epsilon_p$ can be considered as an evaporation rate of total precipitation. Roughly the same factor with the negative sign applied to the convective buoyancy gives the negative buoyancy that drives the downdrafts and gives Eq. (2.11c). It should be emphasized that mesoscale downdrafts can be also accounted for by this term. The dependence of the WISHE instability on ϵ_p has already been investigated by Yano and Emanuel (1991, see their Fig. 2).

b. Nondimensionalization

The M92 organized momentum transport is formulated in terms of nondimensional quantities. Velocity, length, and time are scaled by U_0, H, and H/U_0, re-

[1] The ''cumulus vertical velocity'' may be estimated by dividing w_c by the fractional area σ_c occupied by cumulus convection. For economy, we do not explicitly indicate the factor σ_c.

spectively. We set $U_0 = 10$ m s^{-1}, defined as the strength of the relative inflow to a typical mesoscale organized system (see section 3). We use the same scaling as in M92 and, for convenience, omit δ from the dimensional variables. This gives $\delta\phi = U_0^2\phi$ and $\delta\theta = (U_0^2/\epsilon_k)\theta$ with a corresponding nondimensionalization for the equivalent potential temperature.

The diagnostic equations (2.11c,d) are unaltered. We obtain the nondimensional set of prognostic equations from (2.8a,b), (2.3), (2.10a,b),

$$\frac{D_b}{Dt}\mathbf{v}_b = -\nabla\phi_b - \hat{C}_D|\mathbf{v}_b|\mathbf{v}_b + Q_M, \quad (2.12a)$$

$$\frac{D_m}{Dt}\mathbf{v}_m = -\nabla\phi_m - Q_M, \quad (2.12b)$$

$$\frac{D_t}{Dt}\theta = -\hat{N}w + \dot{Q}_{\text{conv}} - \dot{Q}_R, \quad (2.12c)$$

$$\frac{D_b}{Dt}\theta_{eb} = E - \frac{1}{\delta}D, \quad (2.12d)$$

$$\frac{D_m}{Dt}\theta_{em} = D - \dot{Q}_R, \quad (2.12e)$$

and the following diagnostic equations from (2.2a,c), (2.7a,b), (2.6),

$$\phi_b = -\theta + \phi_t, \quad (2.13a)$$

$$\phi_m = \theta + \phi_t, \quad (2.13b)$$

$$\frac{1}{2}\nabla\cdot\mathbf{v}_b + w = 0, \quad (2.13c)$$

$$\frac{1}{2}\nabla\cdot\mathbf{v}_m + w_t - w = 0, \quad (2.13d)$$

$$\phi_t + \theta = \frac{\hat{S}}{k}w_t. \quad (2.13e)$$

Using (2.5a,b), (2.11a,b), the source terms on the right-hand side of (2.12) are

$$\dot{Q}_{\text{conv}} = \hat{N}w_c, \quad (2.14a)$$

$$\dot{Q}_R = \hat{Q}_{R_0} + \frac{\theta}{\hat{\tau}_R}, \quad (2.14b)$$

$$E = \hat{C}_\theta|\mathbf{v}_b|(\theta^*_{eb} - \theta_{eb}), \quad (2.14c)$$

$$D = (w_d - w_e)(\theta_{eb} - \theta_{em}). \quad (2.14d)$$

We have introduced the following nondimensional parameters:

$$\hat{C}_D = \frac{H}{h_b}C_D = 1.6 \times 10^{-2}, \quad (2.15a)$$

$$\hat{C}_\theta = \frac{H}{h_b}C_\theta = 1.92 \times 10^{-2}, \quad (2.15b)$$

$$\delta = \frac{h_b}{H} = 0.0625, \quad (2.15c)$$

$$\hat{N} = \frac{\gamma C_p N^2 H\theta_0^2(T_b - T_t)}{gU_0^2} = 41.5, \quad (2.15d)$$

$$\hat{Q}_{R_0} = \frac{\epsilon_k H\dot{Q}_{R_0}}{U_0^3} = 1.57 \times 10^{-2}, \quad (2.15e)$$

$$\hat{\tau}_R = \frac{U_0\tau_R}{H} = 5.5 \times 10^3, \quad (2.15f)$$

$$\hat{S} = \frac{NH}{U_0} = 8.0. \quad (2.15g)$$

c. Linearization

In the following analysis, $(\bar{\ })$ designates base-state values and $(')$ the deviation from this state. For convenience, the primes are omitted when there is no likelihood of ambiguity. Unless otherwise stated, all variables are either a mean value or a deviation from the mean. We assume a homogeneous positive (westerly) wind $\overline{u}$ as a mean basic state. The westerly mean state is chosen bearing in mind a westerly wind burst environment in which organized mesoscale systems, whose momentum flux we seek to parameterize, commonly occur. Note that results for the easterly mean wind case can be immediately obtained by reversing the phase velocity and by changing the sign of the mesoscale phase velocity c_M (e.g., making the results applicable to West African squall lines).

We also assume the large-scale mean vertical motion is zero ($\overline{w} = 0$), so the cumulus updraft is exactly compensated by environmental subsidence:

$$\overline{w}_c = -\overline{w}_e. \quad (2.16a)$$

Note that although cumulus updrafts are always more concentrated and vigorous than environmental subsidence, the grid-averaged effect should balance if there is no direct interaction among neighboring grid volumes (as is the case in all GCMs). Due to the assumption that radiative cooling balances the convective heating, we have

$$\overline{w}_c = \hat{Q}_{R0}/\hat{N}. \quad (2.16b)$$

Furthermore, the balance between the environmental descent and the surface flux in the subcloud layer, and radiative cooling in the middle troposphere lead to

$$\theta^*_{eb} - \overline{\theta}_{eb} = \hat{Q}_{R_0}/\delta\hat{C}_\theta|\overline{u}_b|, \quad (2.16c)$$

$$\overline{\theta}_{eb} - \overline{\theta}_{em} = \epsilon_p\hat{N}. \quad (2.16d)$$

We superimpose a small amplitude disturbance on the mean state defined by (2.16a,b,c,d). Using (2.12), the linear equations for the deviations are then

$$\left(\frac{\partial}{\partial t} + \overline{u}_b\frac{\partial}{\partial x} + F\right)u_b = -\frac{\partial}{\partial x}\phi_b + Q_M, \quad (2.17a)$$

$$\left(\frac{\partial}{\partial t} + \overline{u}_m\frac{\partial}{\partial x}\right)u_m = -\frac{\partial}{\partial x}\phi_m - Q_M, \quad (2.17b)$$

$$\left(\frac{\partial}{\partial t} + \overline{u}_t\frac{\partial}{\partial x} + \frac{1}{\hat{\tau}_R}\right)\theta = -\hat{N}w_e, \quad (2.17c)$$

$$\left[\delta\left(\frac{\partial}{\partial t} + \overline{u}_b\frac{\partial}{\partial x}\right) + \alpha_e + \alpha_d\right]\theta_{eb} = \alpha_\theta u_b + \alpha_d\theta_{em} - \lambda(w_d - w_e), \quad (2.17d)$$

$$\left(\frac{\partial}{\partial t} + \overline{u}_m\frac{\partial}{\partial x} + \alpha_d\right)\theta_{em} = \alpha_d\theta_{eb} + \lambda(w_d - w_e) - \frac{\theta}{\hat{\tau}_R}, \quad (2.17e)$$

where

$$F = 2\hat{C}_D|\overline{u}_b| = 3.2 \times 10^{-2}|\overline{u}_b|, \quad (2.18a)$$

$$\alpha_e = \delta\hat{C}_\theta|\overline{u}_b| = 1.2 \times 10^{-3}|\overline{u}_b|, \quad (2.18b)$$

$$\alpha_\theta = \frac{\hat{Q}_{R_0}}{\overline{u}_b}, \quad (2.18c)$$

$$\alpha_d = \frac{\hat{Q}_{R_0}}{\epsilon_p\hat{N}} = 4.2 \times 10^{-3}, \quad (2.18d)$$

$$\lambda = \epsilon_p\hat{N} = 37.4. \quad (2.18e)$$

We assume that the horizontal coordinate x and the wind component u are positive in the eastward direction. We retain the diagnostic equations (2.13). The term proportional to α_θ in the right-hand side of (2.17d) represents the surface heat flux proportional to the surface wind u_b, namely, the WISHE process.

It is convenient to express the momentum equations (2.17a, b) in the terms of barotropic u_t and baroclinic u_c components:

$$\left(\frac{\partial}{\partial t} + \overline{u}_t\frac{\partial}{\partial x}\right)u_t + \overline{u}_c\frac{\partial}{\partial x}u_c = -\frac{\partial}{\partial x}\phi_t - \hat{F}(u_t + u_c), \quad (2.19a)$$

$$\left(\frac{\partial}{\partial t} + \overline{u}_t\frac{\partial}{\partial x}\right)u_c + \overline{u}_c\frac{\partial}{\partial x}u_t = -\frac{\partial}{\partial x}\theta - \hat{F}(u_t + u_c) + Q_M, \quad (2.19b)$$

where

$$u_b = u_t + u_c, \quad (2.20a)$$

$$u_m = u_t - u_c, \quad (2.20b)$$

and

$$\hat{F} = F/2. \quad (2.21)$$

By definition, $u_c > 0$ means a negative value of the vertical shear (i.e., easterly shear). Because of the integral constraint on momentum generation, the mesoscale momentum tendency Q_M appears in the baroclinic component but not in the barotropic component.

We make additional approximations to facilitate analytic tractability. Considering the smallness of the parameters, we can legitimately approximate $1/\hat{\tau}_R \sim \alpha_d \sim \alpha_e \to 0$. We further assume that the subcloud layer is much shallower than the troposphere, namely, $\delta \to 0$. In physical terms the first set of assumptions removes certain linear damping terms, whereas the second assumption means that the subcloud layer instantaneously adjusts to a change induced by the tropospheric dynamics. These limits are identical to those in section 3b(2) of YE. The second assumption was called the ''boundary-layer quasi-equilibrium'' by Raymond (1995) and ''subcloud-layer entropy equilibrium'' by Emanuel (1995).

Hence, (2.17d) reduces to $\alpha_\theta u_b - \lambda(w_d - w_e) = 0$, which means that the wind-induced surface flux is always balanced by downdraft cooling. Downdraft cooling is further related to the cumulus updraft w_c by (2.11c,d). With this approximation, the surface flux uniquely defines the cumulus updraft w_c. After algebraic manipulation employing (2.13c) we obtain

$$w_c = \epsilon_p\left(\frac{\alpha_\theta}{\lambda} - \frac{1}{2}\frac{\partial}{\partial x}\right)u_b. \quad (2.22)$$

The cumulus updraft (w_c) is therefore proportional to the surface wind (u_b). The component of w_c in phase with u_b, represented by the first term in the right-hand side, is the basic mechanism for the WISHE instability. We can remove WISHE by setting $\alpha_\theta = 0$. Note that we do not have to solve the midlevel moisture equation (2.17e) in this limit.

3. Mesoscale momentum flux parameterization

We use the archetypal momentum flux representation of M92, which is an expression for the *total* flux (i.e., mean + deviation). A decomposition of the total flux into a mean and a deviation is not made unless otherwise stated. All quantities are presented in terms of the nondimensionalization introduced in section 2b. We identify the mesoscale variables and parameters by the subscript *M* but otherwise adopt the notation of M92. This model is a paradigm for mesoscale convective system dynamics and provides the momentum transport on a characteristic scale L_M. We use it as a grid-scale to subgrid-scale model of organized momentum flux. Following M92, the model is asymptotically linked to the large-scale (resolved scale) circulation over the distance L_M. Although the theoretical considerations upon which the model is built does not provide an a priori estimate for

L_M, this distance is about 100 km based on observations and numerical model results.

The mesoscale momentum flux divergence is given by M92 in terms of

$$\Upsilon(z) \equiv L_m \frac{\partial}{\partial z}\langle u_M w_M\rangle, \tag{3.1}$$

where $\langle * \rangle$ designates the *total* ensemble average over L_M. In a steady nonrotating system, provided the momentum flux vanishes at top and bottom of the convective layer, horizontal momentum can be redistributed in the vertical, but mean horizontal motion cannot be generated because the vertical integral momentum flux divergence is identically zero (we call this the integral constraint on the momentum flux).

a. Vertically continuous model

In implementing the archetypal model into the large-scale momentum equation, we assume that a typical mesoscale system occupies a fraction (α_M) of a grid domain. Hence, in a vertically continuous system, the mesoscale momentum transport would be implemented as

$$\left(\frac{\partial}{\partial t} + \mathbf{v}\cdot\boldsymbol{\nabla}\right)u + \frac{\partial}{\partial x}\delta\phi = Q_M(z), \tag{3.2a}$$

where the acceleration due to the momentum flux divergence is

$$Q_M(z) = -\alpha_M \frac{\partial}{\partial z}\langle u_M w_M\rangle. \tag{3.2b}$$

By substitution of (3.1) into (3.2b), we obtain

$$Q_M(z) = -\frac{\alpha_M}{L_M}\Upsilon(z).$$

In this definition, x is positive in the direction of propagation of the mesoscale system in a coordinate frame moving along with the mean wind (or equivalently, along a Galilean-transformed coordinate). More generally, assuming that the x coordinate is aligned along the direction of propagation of the disturbance, we can take the sign of the phase velocity c_M into account as

$$Q_M(z) = -\text{sgn}(c_M)\frac{\alpha_M}{L_M}\Upsilon(z). \tag{3.3}$$

When the inflow strength (u_i), scaled by U_0, departs from unity, (3.3) should, strictly speaking, be multiplied by u_i. Apart from an explicit scale analysis in section 4, we allow for this in a simple way through the mesoscale fractional area α_M,

b. Two-layer model

The corresponding expression of Q_M for the two-layer system in (2.17a, b) and (2.19b) is obtained by integrating (3.3) from the bottom to the middle of the atmospheric column to give

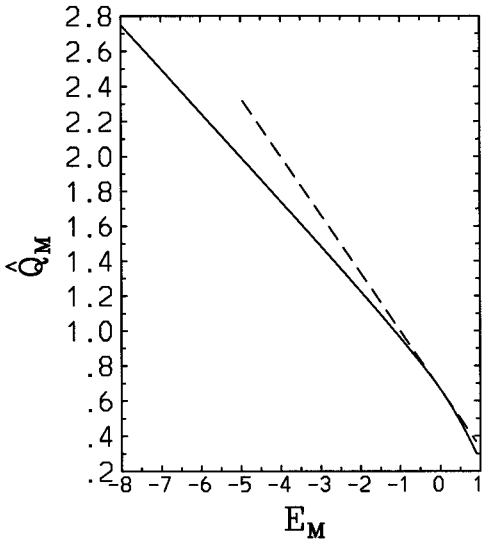

FIG. 2. The rate $\hat{Q}_M$ that the momentum is transported from the upper layer to the lower layer over the scale L_M by the archetypal mesoscale circulation: plotted as a function of the mesoscale pressure jump E_M. The linear approximation around $E_M \sim 0$ is also represented by a dash line.

$$Q_M = \frac{\alpha_M}{L_M}\hat{Q}_M. \tag{3.4a}$$

We have introduced the normalized mesoscale momentum flux divergence

$$\hat{Q}_M \equiv -2\int_0^{1/2} \Upsilon(z)\, dz. \tag{3.4b}$$

The expression for Υ is obtained from Eq. (16) of M92 and substituted into (3.4b). The resulting acceleration, $\hat{Q}_M$, is a function of the nondimensional pressure jump $E_M = 2\alpha_M \Delta p_M / U_0^2$, where Δp_M is a dimensional change of pressure across L_M. The obtained formula (see appendix B) is plotted in Fig. 2. The flux divergence increases and the mesoscale downdraft is stronger for smaller, negative values of E_M (Fig. 2 of M92). In physical terms this corresponds to a *propagating system*; that is, a system that propagates relative to the mean wind at all levels.

As a closure we assume that the mesoscale pressure gradient E_M/L_M is correlated with the large-scale gradient $\partial\delta\phi/\partial x$ by a factor ϵ_M, giving

$$E_M = -2\epsilon_M L_M \,\text{sgn}(c_M)\frac{\partial}{\partial x}\delta\phi. \tag{3.5}$$

Note that the sign of E_M is defined as the change of pressure measured from front-to-rear across the system (see M92). The rationale for the closure is that the archetype is expected to be (asymptotically) continuous with the large-scale pressure field over the distance L_M.

When the mesoscale pressure efficiency parameter ϵ_M is unity, the mesoscale pressure p_M perturbation is continuous with its large-scale counterpart so we expect that $\epsilon_M \sim 1$. A more formal estimate is given in section 4.

It is convenient to linearize $\hat{Q}_M$ with respect to E_M, by referring to appendix B:

$$\hat{Q}_M \approx \frac{2}{3}\left(1 - \frac{E_M}{2}\right).$$

The M92 solution has two physically distinct modes of behavior called *symmetric* and *asymmetric*. The cross-system change of pressure is identically zero in the symmetric mode, in contrast with the nonzero pressure change in the asymmetric mode. Nevertheless, the symmetric mode is nontrivial because it overturns the fluid (i.e., a nonzero mass transport and momentum flux). In other words, $\hat{Q}_M \neq 0$ even if $E_M = 0$. The asymmetric mode becomes identical to the symmetric mode for the special case of $E_M = 0$, which also has a nondegenerate momentum flux. By substitution into (3.4a) and using (3.5),

$$Q_M \approx \frac{2\ \mathrm{sgn}(c_M)\alpha_M}{3L_M} + \frac{2\alpha_M\epsilon_M}{3}\frac{\partial}{\partial x}\delta\phi.$$

We now divide Q_M into mean and deviation parts, namely

$$\overline{Q}_M = \frac{2\ \mathrm{sgn}(c_M)\alpha_M}{3L_M}, \tag{3.6a}$$

$$Q'_M = \frac{2\alpha_M\epsilon_M}{3}\frac{\partial}{\partial x}\delta\phi'. \tag{3.6b}$$

In physical terms, once a large-scale disturbance is created (in our framework as a Kelvin-like wave disturbance but in general terms by a variety of mechanisms), we envisage that mesoscale organized systems occur and move at a characteristic phase speed c_M. For example, organized mesoscale convective systems occur within superclusters in the tropical Western Pacific (Moncrieff and Klinker 1997; Figs. 1 and 2) and squall lines within easterly waves in West Africa. Equation (3.6a) essentially represents a homogeneous feedback of the mesoscale organization to the large-scale flow. In the following linear perturbation analysis, the term (3.6b) will be incorporated into (2.17a,b) and (2.19b).

4. Shallow-water limit

The two-layer system introduced in section 2 contains two limiting cases based on the upper-level stratification $\hat{S}$. First, when $\hat{S} \to 0$, in which case $\phi_m = 0$ follows from (2.13e), there is no pressure disturbance and no flow in the upper layer (i.e., $u_m = 0$). This corresponds to a strong wave absorption at the top of the atmosphere, which we call the *sponge-layer limit*. A more useful one is $\hat{S} \to \infty$, which is the *shallow-water limit* used by YE. We have $w_t, = 0$ from (2.13e), which further implies $u_t = 0$ from (2.13c,d). The perturbation is completely baroclinic provided there is no mean vertical shear ($\overline{u}_c = 0$). We now consider this limit in detail by setting $u_b = u_c$, $\overline{u}_b = \overline{u}_t$.

We assume a wave solution of the form $\exp[ik(x - ct)]$, where $c = c_r + ic_i$ is a complex phase velocity consisting of the real phase velocity c_r and the imaginary part c_i, which gives the growth rate $\sigma = kc_i$. We obtain

$$(\overline{u}_t - c)u_c = \theta + \frac{Q_M}{ik} - \frac{\hat{F}}{ik}u_c, \tag{4.1a}$$

$$(\overline{u}_t - c)\theta = \tilde{N}^* u_c. \tag{4.1b}$$

The complex stratification

$$\tilde{N}^* = \frac{(1 - \epsilon_p)\hat{N}}{2} + \frac{\alpha_\theta}{ik} \tag{4.2}$$

is an expression for the thermodynamic modification due to a combination of the surface heat flux and moist convection (i.e., WISHE effect) defined by using (2.22). The nonzero imaginary part means that the positive temperature anomaly slightly lags the positive wind anomaly when the WISHE parameter α_θ is nonzero.

We now consider the effect of the mesoscale momentum transport under the pressure closure (3.6b). In the shallow-water limit, the mesoscale pressure perturbation $E_M/2$ is assumed to be proportional to the potential temperature by setting $\delta\phi' = -\theta$ in (3.6b). By substitution, the sum of the pressure gradient and the mesoscale momentum source terms gives

$$\theta + \frac{Q_M}{ik} = \left(1 - \frac{2}{3}\tilde{\alpha}_M\right)\theta, \tag{4.3}$$

where the *effective* mesoscale fractional area $\tilde{\alpha}_M \equiv \epsilon_M\alpha_M$ has been introduced. Equation (4.3) means that the effective pressure force changes from $\nabla\theta$ to $(1 - 2\tilde{\alpha}_M/3)\nabla\theta$ through the action of the mesoscale momentum flux divergence. This reduces the *effective* stratification from $\hat{N}$ to $(1 - 2\tilde{\alpha}_M/3)\hat{N}$ and also reduces the complex stratification $\tilde{N}^*$ defined by (4.2). The reduction of the effective stratification stems from the fact that a stronger mesoscale pressure change from front-to-rear of the mesoscale system (i.e., $E_M < 0$) accelerates the low-level flow in the direction of propagation of the mesoscale organization [cf. (3.6b)], aided by a stronger mesoscale downdraft (cf. Fig. 2 of M92). This counteracts the large-scale pressure force, which then decelerates the low-level flow in the direction of propagation.

By taking the determinant of (4.1a,b) and substituting (4.3) we obtain the complex dispersion equation

$$c = \overline{u}_t + \frac{\hat{F}}{2ik} \pm \left[-\frac{\hat{F}^2}{4k^2} + \left(1 - \frac{2}{3}\tilde{\alpha}_M\right)\tilde{N}^*\right]^{1/2}. \tag{4.4}$$

A positive growth rate occurs when the square root is of sign opposite to the mean flow. An unstable WISHE disturbance therefore propagates upwind (relative to the

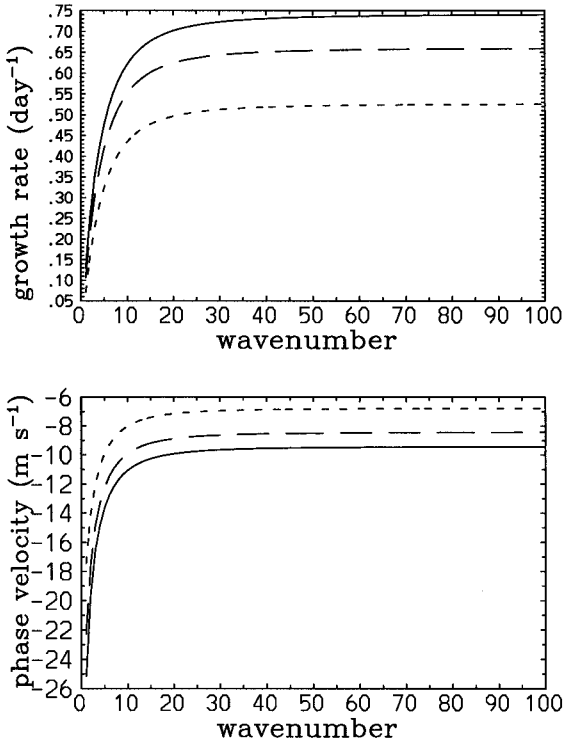

FIG. 3. The modification of the WISHE instability by mesoscale momentum transport. The growth rate (day^{-1}: upper frame) and the phase velocity (m s^{-1}: lower frame) are plotted against the global longitudinal wavenumber ($k = 100$ corresponds to a wavelength of 400 km). The solid curve shows the standard case ($\overline{u}_b = 5$ m s^{-1}) without momentum transport. The long-dash and the short-dash curves show the cases with $\tilde{\alpha}_M = 0.2$ and 0.5, respectively.

surface wind) because the stronger wind enhances the surface flux and increases the generation of available potential energy for convection. Therefore both low-level convergence and convection shifts in this direction. This upwind propagation mechanism is illustrated in Fig. 1 of Emanuel (1987) and is a characteristic signature of WISHE.

We now consider the zero surface friction limit $\hat{F} \to 0$ (i.e., $\hat{C}_D \to 0$) in order to simplify the expression. As shown by YE, both the growth rate and the phase velocity asymptotically approach constant values in the high wavenumber limit (cf. Fig. 3 below). This is basically due to the convective downdraft. The effect of the momentum transport on the WISHE instability is readily seen in this limit ($k \to \infty$), in which case,

$$\sigma \to \frac{\varepsilon_p \alpha_\theta}{\lambda}\left[\frac{1}{2}\left(1 - \frac{2}{3}\tilde{\alpha}_M\right)\frac{\tilde{N}}{1 - \epsilon_p}\right]^{1/2}, \quad (4.5a)$$

$$(\overline{u}_t - c_r) \to \left[\frac{(1 - \epsilon_p)}{4}\left(1 - \frac{2}{3}\tilde{\alpha}_M\right)\hat{N}\right]^{1/2}. \quad (4.5b)$$

The growth rate σ is proportional to the WISHE parameter α_θ. The reduction of the effective stratification by the *pressure-driven* mesoscale momentum transport results in a decreased growth rate and reduced phase velocity of WISHE, provided $1 > 2\tilde{\alpha}_M/3$. The reduction of the phase velocity is explained in terms of a slower-moving internal gravity wave associated with a weaker (effective) stratification. In order to understand the reduction of the growth rate, it needs to be appreciated that the WISHE instability is produced through a redistribution of tropospheric mass, as expressed by the thermodynamic equation (4.1b). The adjustment of the atmosphere toward convective neutrality, responding to the wind-induced subcloud-layer moisture anomaly, gives rise to such an effect [Eq. (2.22)]. Hence, the WISHE instability is amplified by a stronger effective density stratification $(1 - 2\tilde{\alpha}/3)\hat{N}$ and vice versa.[2]

A more fundamental change occurs if the threshold $\tilde{\alpha}_M = 3/2$ is exceeded; that is, if the *effective stratification* $(1 - 2\tilde{\alpha}_M/3)\hat{N}$ of the atmosphere changes sign, leading to an *unconditional* thermodynamic instability. Physically, this will occur when the magnitude of the pressure-driven momentum transport exceeds the direct pressure forcing. This occurs if the mesoscale downdraft is sufficiently strong. Note that the *propagating* organized system commonly has a strong downdraft (see M92, Fig. 2). The degree to which this can be realized can be assessed by the following scale analysis. Recall that the effective mesoscale fractional area is defined by $\tilde{\alpha}_M = \epsilon_M \alpha_M u_i$, with explicit reference to the inflow strength u_i. The mesoscale dynamical efficiency ϵ_M is estimated as $\epsilon_M \equiv |\nabla \Delta p_M|/|\nabla \delta p_L| \sim L/L_M(\Delta p_M/\delta p_L)$, where L is the scale of the large-scale disturbance and δp_L is the large-scale pressure anomaly. In terms of the mesoscale fractional area α_M, we need separate considerations for the large-scale and the mesoscale limits.

In the *large-scale limit* where $L \gg L_M$, we expect that α_M is independent of L. We further assume in this limit that $\Delta p_M \sim \delta p_L$ and $u_i \sim 1$. Hence, $\tilde{\alpha}_M \sim (L/L_M)\alpha_M > 1$ is required to achieve an effective unstable stratification. We estimate $L > L_M/\alpha_M \sim 10^4$ km if $L_M \sim 100$ km and $\alpha_M \sim 10^{-2}$. This implies that the unstable stratification may be realized through the action of a planetary-scale disturbance containing an ensemble of mesoscale systems. This is a plausible interaction of organized convection with the Madden–Julian oscillation.

On the other hand, in the *small-scale limit* we expect that the fractional area occupied by the mesoscale convection scales as $\alpha_M \sim (L_M/L)^2$ by assuming that a single mesoscale system occupies an entire grid domain. By substitution, we obtain $\tilde{\alpha}_M \sim (L_M/L)u_i\,\Delta p_M/\delta p_L$. Therefore, $\tilde{\alpha}_M$ is larger at small scales in this limit. When we take the *mesoscale limit* $L \to L_M$, we identify two sce-

[2] This should not be confused with the moisture stratification measured by λ, which has the opposite effect through suppressing instability through the downdraft effect (cf. Fig. 4 of YE). Also note that the "total" downdraft $(w_d - w_e)$ is proportional to $1/\epsilon_p$ [cf. Eq. (2.11c), d].

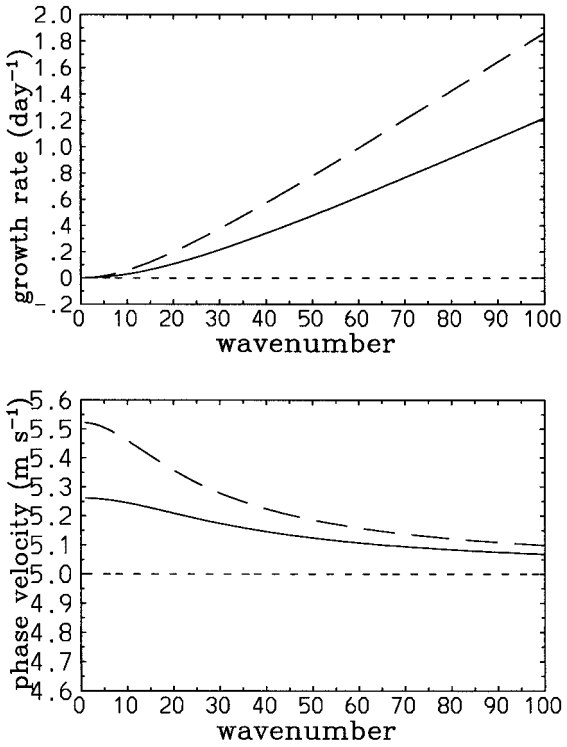

FIG. 4. As in Fig. 3 but for $\tilde{\alpha}_M = 1.5$, 1.51, and 1.52 with the short-dash, the solid, and the long-dash curves, respectively. The effective unstable stratification is created by the mesoscale convective momentum transport with $\tilde{\alpha}_M > 1.5$.

narios for realizing $\tilde{\alpha}_M > 1$; that is, either $\Delta p_M/\delta p_L > 1$ or $u_i > 1$. Consequently, the mesoscale momentum transport can self-induce an effective unstable stratification if there is a sufficiently large pressure disturbance and/or a strong relative inflow. We refer to this instability as the effective convective instability by mesoscale momentum transport (CIMMT).

We plot the direct numerical results from (4.4) in Figs. 3 and 4 without the limit of $F \to 0$. For simplicity, we do not consider the scale dependence of $\tilde{\alpha}_M$. Below the threshold $\tilde{\alpha}_M < 3/2$ (Fig. 3), both the growth rate and the absolute phase velocity decrease as $\tilde{\alpha}_M$ increases. This is to be expected from (4.5a,b): the cases with $\tilde{\alpha}_M = 0$, 0.2, and 0.5 are shown by the solid, the long-dash, and the short-dash curves. At the threshold $\tilde{\alpha}_M = 3/2$ (short-dash curve in Fig. 4), the disturbance is neutral and purely advected by the zonal wind. Above the threshold $\tilde{\alpha}_M > 3/2$, the disturbance is again destabilized and grows faster at smaller scales, which is typical of convective instabilities. The growth rate is sensitive to $\tilde{\alpha}_M$. Only a slightly higher value than the threshold ($\tilde{\alpha}_M = 1.51$ and 1.52 by the solid and long-dash curves in Fig. 4, respectively) provides a much larger growth than the WISHE mode, ostensibly due to a fast timescale represented by the Väisälä frequency $\overline{N}$. Note that above this threshold the disturbance propagates *downwind* in contrast to the WISHE instability.

The faster growth rate for the smaller scale under CIMMT is compatible with a scale analysis, which suggests that a mesoscale convective system can be self-induced by this instability. It is emphasized that the fastest growth rate in the smallest scale in this scenario does not contradict the scale separation principle. Note that Moncrieff's archetypal model does not strictly rely on this principle per se, because it predicts the *total* momentum flux, not the eddy perturbations which follow from the Reynolds averaging approach. In other words, the archetypal model represents a coherent structure rather than an ensemble of quasi-random fluctuations.

5. Conclusions

The impact of mesoscale momentum transport on the dynamics of the Tropics was assessed through a linear analysis of the analogue shallow-water atmospheric model of Yano and Emanuel (1991). In order to simplify the analysis, the model contained only a Kelvin-type wave mode. Furthermore, the subcloud layer is assumed to adjust instantaneously to tropospheric changes, which closes the mass flux representation for the thermodynamic effects of ordinary cumulus convection.

The mesoscale momentum flux, as formulated by the Moncrieff (1992) archetypal dynamical model that approximates squall-line-like cloud systems, was incorporated in an idealized large-scale model of the tropical atmosphere. For the closure, we assumed that the mesoscale momentum flux is proportional to the large-scale pressure wave perturbation (consistent with the archetypal formulation). The action of mesoscale momentum transports was found to reduce both the growth rate and phase velocity of the WISHE mode.

A reduced phase speed for large-scale convectively driven disturbances in the tropical atmosphere is an attractive feature. Most linear theories, including those based on WISHE (Yano et al. 1995), produce a much faster propagation than is realistic for cloud clusters, superclusters, and Madden–Julian waves. From a linear analysis and numerical experiments, respectively, Wang and Rui (1990) and Salby et al. (1994) proposed that surface friction reduces the phase speed of the large-scale disturbances. Although our result indirectly invokes surface fluctuations, the reduction of phase speed is due primarily to convective momentum transport. This implies that the propagation of superclusters may be partly controlled by the intensity of organized mesoscale convection within them.

Furthermore, it is inferred that the large-scale *effective* stratification can be *absolutely* destabilized, provided the mesoscale momentum transport is sufficiently strong (the effective convective instability by mesoscale momentum transport, CIMMT). A scale analysis suggests that this instability may be realized not only at the mesoscale limit (if the perturbations are sufficiently intense) but also at larger scales (provided the large-scale

disturbances contain a sufficiently large population of mesoscale convective systems). Thus its impact on Madden–Julian waves warrants further study.

Based on these results, momentum transport by organized convection has an identifiable effect on large-scale tropical dynamics and the responsible mechanisms have been quantified. While more realistic models are certainly required, our conclusions point to a potential future issue for general circulation models when the horizontal resolution improves beyond a certain threshold (guaranteed by inevitable advances in computer power). Arguably, this juncture has already been reached because state-of-the-art global weather forecasting models sometimes attempt to explicitly treat the largest tropical organized cloud systems (superclusters) as identified by Moncrieff and Klinker (1997).

We caution that our idealized study should be regarded as preliminary because of the simple shallow-water analogue linear model and the omission, for example, of a more explicit description of the thermodynamic effects of mesoscale downdrafts or the convective life-cycle scheme of Yano et al. (1995, 1996, 1997).[3] Either could substantially modify the large-scale thermodynamics. On the other hand, the idealized approach enabled us to isolate pertinent dynamical mechanisms. The results also suggest that the mesoscale momentum flux, which is a distinguishing feature of organized precipitating convection, should be given serious attention. In order to strengthen and quantify this conclusion, we plan to report the full two-layer linear analysis in the near future and to perform cloud-resolving numerical experiments to ascribe more realism to the results.

Acknowledgments. The major part of the work was performed when J.I.Y was a visitor at NCAR during July–September 1995. J.I.Y is supported by the Australian Government Cooperative Research Centre's Program.

APPENDIX A

List of Symbols

$C_D = 1 \times 10^{-3}$	surface drag coefficient
$\hat{C}_D$	surface drag coefficient [nondimensional, Eq. (2.15a)]
$C_\theta = 1.2 \times 10^{-3}$	evaporation rate by wind
$\hat{C}_\theta$	evaporation rate by wind [nondimensional, Eq. (2.15b)]
c_M	phase velocity for the mesoscale convective system (along the coordinate moving with the vertical-mean wind)
D_b/Dt	Lagrangian time derivative for the lower layer [Eq. (2.9a)]
D_m/Dt	Lagrangian time derivative for the upper layer [Eq. (2.9b)]
D_t/Dt	Lagrangian time derivative advected by a mean tropospheric wind v_t [Eq. (2.4)]
E_M	nondimensional mesoscale pressure jump
F	nondimensional surface friction rate [Eq. (2.18a)]
$\hat{F}$	modified nondimensional surface friction rate [Eq. (2.21)]
$H = 8$ km	depth of troposphere (density-weighted scale in log-p coordinate). Also used as the length scale for the nondimensionalization.
h	mesoscale downdraft depth in Moncrieff's archetypal model
h_0	inflow depth of the front-to-rear flow in Moncrieff's archetypal model
$h_b = 500$ m	depth of subcloud layer
L	scale of the large-scale disturbance
L_M	horizontal extent of the mesoscale system
$\hat{N}$	nondimensional stratification [Eq. (2.15d)]
p_L	low-level large-scale pressure
p_M	mesoscale pressure
$\dot{Q}_{\text{conv}}$	convective heating
Q_M	momentum redistribution by the mesoscale circulation
$\overline{Q}_M$	homogeneous part of the momentum redistribution
Q'_M	deviation of the momentum redistribution
$\hat{Q}_M$	normalized momentum redistribution [Eq. (3.4b)]
$\dot{Q}_R$	radiative cooling by long wave radiation
$\hat{Q}_{R0}$	nondimensional cooling rate of the atmosphere [Eq. (2.15e)]
$\hat{S}$	upper-level stratification [nondimensional, Eq. (2.15g)]
$T_b = 300$ K	temperature at the top of subcloud layer
T_t	temperature averaged over the troposphere
$U_0 = 10$ m s^{-1}	strength of the relative inflow to the mesoscale organized system used as a velocity scale
u_b	lower-layer wind disturbance (westerly)
$\overline{u}_b$	lower-layer mean wind (westerly)
u_c	baroclinic wind disturbance [westerly, Eq. (2.20)]
$\overline{u}_c$	baroclinic mean wind [westerly, Eq. (2.20)]
u_i	inflow strength in Moncrieff's archetype

[3] This was originally called the grid column scheme in Yano et al. (1995, 1996).

u_m upper-layer wind disturbance (westerly)
$\overline{u}_m$ upper-layer mean wind (westerly)
u_t barotropic wind disturbance [westerly, Eq. (2.20)]
$\overline{u}_t$ barotropic mean wind [westerly, Eq. (2.20)]
$\mathbf{v}_m$ upper-layer wind vector, defined at the midlevel
$\mathbf{v}_t$ mean tropospheric wind vector, barotropic wind
w vertical velocity at the middle troposphere
w_c total cumulus updraft
w_d convective downdraft
w_e environmental subsidence
α_d nondimensional downdraft damping rate [Eq. (2.18d)]
α_e nondimensional evaporative damping rate [Eq. (2.18b)]
α_M fractional area occupied by the mesoscale convective systems
$\tilde{\alpha}_M$ effective mesoscale fractional area
α_θ WISHE parameter [nondimensional evaporation rate by wind, Eq. (2.18c)]
$\gamma = \Gamma_d/\Gamma_m = 1.7$ the ratio of dry to moist adiabatic lapse rates
Δp_M dimensional change of the pressure crossing over the whole domain of the mesoscale organization
δ nondimensional depth of subcloud layer [Eq. (2.15c)]
δp_L large-scale pressure anomaly
$\delta\alpha$ perturbation specific volume
ϵ_k thermodynamic efficiency [Eq. (2.2b)]
ϵ_M mesoscale pressure efficiency parameter
$\epsilon_p = 0.9$ ''precipitation efficiency'' coefficient
θ_{eb} equivalent potential temperature of the subcloud layer
θ^*_{eb} saturated equivalent potential temperature of the subcloud layer
θ_{em} equivalent potential temperature at the midtroposphere
λ nondimensional cooling rate by downdraft [Eq. (2.18e)]
$\tau_R = 50$ day longwave radiative relaxation time (constant for Newtonian cooling term)
$\hat{\tau}_R$ longwave radiative relaxation time [nondimensional, Eq. (2.15f)]
ϕ_b subcloud-layer geopotential
ϕ_t geopotential averaged over the troposphere
ϕ_m midlevel geopotential
Υ momentum flux divergence due to the mesoscale circulation [Eq. (3.1)]

APPENDIX B

Explicit Formula for $\hat{Q}_M$

Explicit formula for $\hat{Q}_M$ defined by Eq. (3.4b) is given by

$$\hat{Q}_M = \begin{cases} \dfrac{1}{2}\left(1 - \dfrac{E}{2}\right) - \dfrac{1-E}{6}\left[h + \dfrac{(1-h)^3}{h^2}\right], & \left(h_0 \geq h \geq \dfrac{1}{2}\right) \\ \dfrac{1}{2}\left(1 - \dfrac{E}{2}\right) - \dfrac{1}{6}\left[1 - h_0 + \dfrac{h_0^3}{(1-h_0)^2}\right], & \left(\dfrac{1}{2} \geq h_0 > h\right), \end{cases}$$

where

$$h = \frac{1}{4}\{3 - (1-E)^{-1/2}\},$$

$$h_0 = \frac{1}{4}\{1 + (1-E)^{1/2}\}.$$

REFERENCES

Emanuel, K. A., 1987: An air–sea interaction model of intraseasonal oscillations in the tropics. *J. Atmos. Sci.,* **44,** 2324–2340.

——, 1995: The behavior of a simple hurricane model using a convective scheme based on subcloud-layer entropy equilibrium. *J. Atmos. Sci.,* **52,** 3960–3968.

——, J. D. Neelin, and C. S. Bretherton, 1994: On large-scale circulations in convecting atmospheres. *Quart. J. Roy. Meteor. Soc.,* **120,** 1111–1143.

Houze, R. A., Jr., 1989: Observed structure of mesoscale convective systems and implications for large-scale heating. *Quart. J. Roy. Meteor. Soc.,* **115,** 425–461.

——, and A. K. Betts, 1981: Convection in GATE. *Rev. Geophys. Space Phys.,* **19,** 541–576.

——, S. A. Rutledge, M. I. Biggerstaff, and B. F. Smull, 1989: Interpretation of Doppler weather radar displays of midlatitude mesoscale convective systems. *Bull. Amer. Meteor. Soc.,* **70,** 608–619.

Klemp, J. B., and D. R. Durran, 1983: An upper boundary condition permitting internal gravity wave radiation in numerical mesoscale models. *Mon. Wea. Rev.,* **111,** 430–444.

Lafore, J.-P., and M. W. Moncrieff, 1989: A numerical investigation

of the organization and interaction of the convective and stratiform regions of tropical squall lines. *J. Atmos. Sci.,* **46,** 521–544.

——, J.-L. Redelsperger, and G. Jaubert, 1988: Comparison between a three-dimensional simulation and Doppler radar data of a tropical squall line: Transports of mass, momentum, heat, and moisture. *J. Atmos. Sci.,* **45,** 3483–3500.

Laing, A. G., and J. M. Fritsch, 1997: The global population of mesoscale convective complexes. *Quart. J. Roy. Meteor. Soc.,* **123,** 3483–3500.

LeMone, M. A., and M. W. Moncrieff, 1994: Momentum and mass transport by convective bands: Comparisons of highly idealized dynamical models to observations. *J. Atmos. Sci.,* **51,** 281–305.

Liu, C., and M. W. Moncrieff, 1996: Mass and momentum transports by organized convection: Effects of shear and buoyancy. *J. Atmos. Sci.,* **53,** 964–979.

Madden, R. A., and P. R. Julian, 1971: Detection of a 40–50 day oscillation in the zonal wind in the tropical Pacific. *J. Atmos. Sci.,* **28,** 702–708.

Moncrieff, M. W., 1981: A theory of organized steady convection and its transport properties. *Quart. J. Roy. Meteor. Soc.,* **107,** 29–50.

——, 1992: Organized convective systems: Archetypal dynamical models, mass and momentum flux theory, and parameterization. *Quart. J. Roy. Meteor. Soc.,* **118,** 819–850.

——, 1995: Mesoscale convection from a large-scale perspective. *Atmos. Res.,* **35,** 87–112.

——, 1997: Momentum transport by organized convection. *The Physics and Parameterization of Moist Convection.* NATO Advanced Study Series C: Mathematics and Physical Sciences, Kluwer, in press.

——, and E. Klinker, 1997: Mesoscale cloud systems in the Tropical Western Pacific as a process in general circulation models. *Quart. J. Roy. Meteor. Soc.,* **123,** 805–827.

Neelin, J. D., I. M. Held, and K. H. Cook, 1987: Evaporation–wind feedback and low-frequency variability in the tropical atmosphere. *J. Atmos. Sci.,* **44,** 2341–2348.

Raymond, D. J., 1995: Regulation of moist convection over the warm tropical oceans. *J. Atmos. Sci.,* **52,** 3945–3959.

Rutledge, S. A., 1991: Middle latitude and tropical mesoscale convective systems. *Rev. Geophys. Suppl.,* **29,** 88–97.

Salby, M. L., R. R. Garcia, and H. H. Hendon, 1994: Planetary-scale circulations in the presence of climatological and wave-induced heating. *J. Atmos. Sci.,* **51,** 2344–2367.

Wang, B., and H. Rui, 1990: Dynamics of the coupled moist Kelvin–Rossby wave on an equatorial β plane. *J. Atmos. Sci.,* **47,** 397–413.

Wu, X., and M. W. Moncrieff, 1996: Collective effects of organized convection and their approximation in general circulation models. *J. Atmos. Sci.,* **53,** 1477–1495.

Yanai, M., and R. H. Johnson, 1993: Impacts of cumulus convection on thermodynamic fields. *The Representation of Cumulus Convection in Numerical Models, Meteor. Monogr.,* No. 46, Amer. Meteor. Soc., 39–62.

Yano, J. I., and K. A. Emanuel, 1991: An improved model of the equatorial troposphere and its coupling with the stratosphere. *J. Atmos. Sci.,* **48,** 377–389.

——, J. C. McWilliams, M. W. Moncrieff, and K. A. Emanuel, 1995: Hierarchical tropical cloud systems in an analog shallow-water model. *J. Amos. Sci,* **52,** 1723–1742.

——, ——, and M. W. Moncrieff, 1996: Fractality in idealized simulations of large-scale tropical cloud systems. *Mon. Wea. Rev.,* **124,** 838–848.

——, M. W. Moncrieff, and J. C. McWilliams, 1998: Linear stability and single-column analysis of several parameterization categories in a shallow-water model. *Quart. J. Roy. Meteor. Soc.,* in press.